ACS APPLIED MATERIALS & INTERFACES

Research Article

www.acsami.org

Nerve Guidance Conduits from Aligned Nanofibers: Improvement of Nerve Regeneration through Longitudinal Nanogrooves on a Fiber Surface

Chen Huang,[†] Yuanming Ouyang,*[,†,‡] Haitao Niu,[§] Nanfei He,[†] Qinfei Ke,[†] Xiangyu Jin,[†] Dawei Li,[†] Jun Fang,[†] Wanjun Liu,[†] Cunyi Fan,[‡] and Tong Lin*[,§]

[†]Key Laboratory of Textile Science and Technology, College of Textiles, Donghua University, Shanghai 201620, China

[‡]Department of Orthopaedic Surgery, the Affiliated Sixth People's Hospital, Shanghai Jiaotong University, Shanghai 200233, China

[§]Institute for Frontier Materials, Deakin University, Geelong, Victoria 3216, Australia

Supporting Information

ABSTRACT: A novel fibrous conduit consisting of well-aligned nanofibers with longitudinal nanogrooves on the fiber surface was prepared by electrospinning and was subjected to an *in vivo* nerve regeneration study on rats using a sciatic nerve injury model. For comparison, a fibrous conduit having a similar fiber alignment structure without surface groove and an autograft were also conducted in the same test. The electrophysiological, walking track, gastrocnemius muscle, triple-immunofluorescence, and immunohistological analyses indicated that grooved fibers effectively improved sciatic nerve regeneration. This is mainly attributed to the highly ordered secondary structure formed by surface grooves and an increase in the specific surface area. Fibrous conduits made of longitudinally aligned nanofibers with longitudinal nanogrooves on the fiber surface may offer a new nerve guidance conduit for peripheral nerve repair and regeneration.

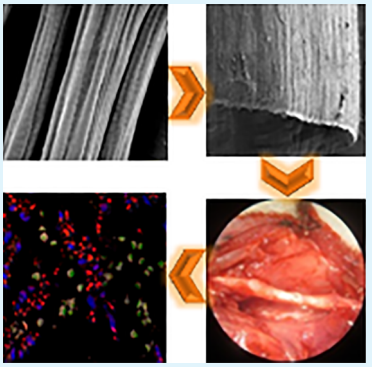

KEYWORDS: *groove, nanofibers, electrospinning, nerve guidance conduit, nerve regeneration, tissue engineering*

INTRODUCTION

Nerve injury caused by accidents or diseases is an important clinical issue. Nerve damage with a short gap (e.g., 1−2 mm) can be repaired usually by end-to-end suture, while the nerve often loses its regeneration and recovery capability when the lesion gap is longer.[1] The most efficient treatment so far to the nerve injuries, which are unrepairable by direct end-to-end suture, is autologous nerve grafting. Autologous nerve grafting, however, has disadvantages including a shortage of nerve donor, multiple rounds of surgery, and function loss at the donor site.[2,3]

Substantial attention has been devoted recently to the repair and regeneration of nerves through tissue engineering. Neural tissue engineering involves the outgrowth of nerves in artificial nerve guidance conduits (NGCs). It has been identified as the major alternative strategy to nerve repair and regeneration. As a key part for neural tissue engineering, NGCs are expected to provide appropriate physical and chemical cues to direct cell migration toward a targeted function. Recent papers indicated that cell migration was mainly controlled by the physical aspects although both physical structure (i.e., channels formed by aligned nanofibers or micropatterned films) and chemical/biological agents (i.e., growth factors) facilitate cell adhesion and differentiation.[4−12]

Nanofibers, mostly produced by an electrospinning technique, show great potential for NGC applications, since they have small diameter, large surface-to-volume ratio, and a similar morphology to native extracellular matrices.[13] NGCs with well-controlled nanofiber alignment structure is highly desirable. It was reported that neurite outgrowth could be exquisitely controlled by surface property and alignment of fibers.[16] Some aligned nanofibers can even regulate the preferential differentiation of neural stem cells.[17,18] Therefore, NGCs with a longitudinal fiber alignment are expected to accelerate nerve cell growth along the conduit.

Several methods have been employed to prepare nanofiber conduits. Early work used a "roll & seal" method to prepare fibrous conduits, in which an aligned nanofiber membrane was electrospun, followed by cutting into a strip, formed into a tube structure, and finally fixed with a suture.[19,20] This method has seldom been used in recent years, because the sutured structure is unstable and contains seams. Conduits were also prepared by mounting micro- or nanofibers to the inner wall of a dense polymer/protein tube. In this case, the conduit was impermeable and fibers inside the conduit functioned mainly to guide cell growth.[21,22] Recently, fibrous conduits were prepared mainly by directly electrospinning polymer solution into a conduit. Conduits with circumferentially aligned

Received: January 2, 2015
Accepted: March 18, 2015
Published: March 18, 2015

DOI: 10.1021/am509227t
ACS Appl. Mater. Interfaces 2015, 7, 7189−7196

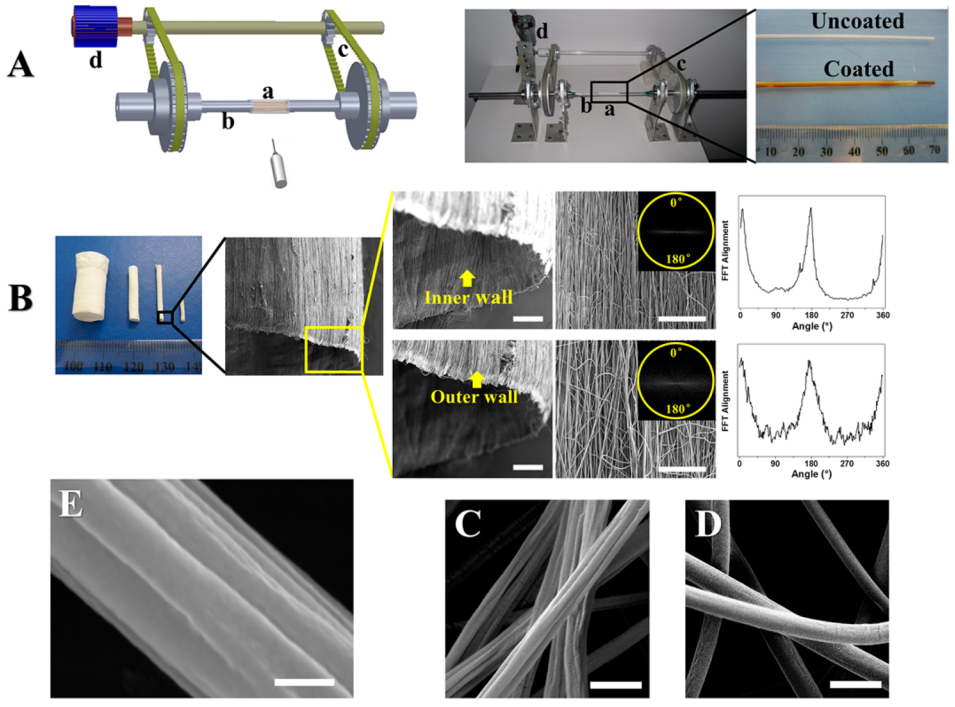

Figure 1. (A) Schematic diagram and photo of the fiber conduit electrospinning setup, (B) digital photo, SEM images, and 2D FFT alignment plots of CAB nanofibrous conduits; SEM images of nanofibers electrospun from (C) high molecular CAB ($M_w \approx 70\,000$), (D) low molecular CAB ($M_w \approx 30\,000$), and (E) a single grooved CAB fiber. (Scale bars in B = 100 μm, C and D = 1 μm, and E = 200 nm.)

nanofibers have been prepared by depositing as-electrospun nanofibers onto a high-speed roller,[14,15] and conduits with longitudinally aligned nanofibers were also prepared by using nonrotating collectors such as two poles[23] or a pair of uniaxially arranged pin electrodes[24] and two rotating electrodes.[25] However, longitudinally aligned nanofiber conduits prepared using two isolated electrodes are often limited to a short length because aligned fibers in a long tube are easy to collapse into fiber bundles.

Fiber diameter and surface morphology are also important parameters affecting cell growth in NGCs. Nanofibers facilitate cell growth and promote functional recovery of peripheral nervous systems.[26−29] However, when fibers are finer than 100 nm, cell adhesion is restrained due to the focal adhesion cues being too small to be recognized.[30,31] The majority of studies on nanofiber-based NGCs are based on nanofibers with a smooth surface. Effects of fiber surface morphology on the nerve repair performance of nanofibrous NGCs have not often been reported in research literature.

In our previous study, we have developed an effective method to electrospin nanofibers with multiple longitudinal grooves and also proved that this ordered secondary structure can considerably enhance the growth of nerve cells *in vitro*, even if the fibers are in a randomly orientated state.[32] In this study, we develop a novel technique to directly electrospin nanofibers into a fibrous NGC and control the nanofibers to align along the longitudinal direction. By using cellulose acetate butyrate (CAB) as model polymer, the nanofibers in the NGCs can have either a smooth surface or nanosized longitudinal grooves on the surface, depending on the molecular weight of the polymer used for electrospinning. This allows us to evaluate the effect of the secondary alignment structure on nerve growth *in vivo*. Our *in vivo* results on rats using a sciatic nerve injury model have indicated that surface grooves on nanofibers considerably enhance nerve regeneration. Since CAB has good biocompatibility,[33] CAB fibrous conduits made of longitudinally aligned nanofibers with longitudinal nanogrooves on the fiber surface may offer a new nerve guidance conduit for peripheral nerve repair and regeneration.

EXPERIMENTAL SECTION

Materials. Cellulose acetate butyrates (CAB) with molecular weight $M_v \approx 70\,000$ and $M_v \approx 30\,000$ and poly(ε-caprolactone) (PCL) were obtained from Sigma-Aldrich. Polyurethane (PEU) was obtained from the Dow Chemical Company. Poly(lactic acid-*co*-glycolic acid) (PLGA, PLA/PGA = 85:15, molecular weight 150 000 Da) was purchased from Jinan Daigang Biomaterial Co., Ltd. Acetone (Chem-Supply), *N*,*N*′-dimethylformamide (DMF, Chem-Supply), and 1,1,1,3,3,3-hexafluoroisopropanol (HFP, Fluorochem) are of reagent grade. All other reagents used for biomedical experiments were from Gibco Life Technologies, USA. Polymer solutions for electrospinning were prepared by dissolving polymer in the respective solvent. For CAB, two solutions were prepared, one from high M_v (70 000) CAB with a concentration of 15% w/w, and another from lower M_v (30 000) with a concentration of 30% w/w. Both solutions used a mixture of acetone/DMF (3:1, v/v) as solvent. PEU (10% w/w) was in a solvent mixture of acetone/DMF (1:1, v/v); PCL (12% w/w) and PLGA (12% w/w) were in HFP.

Electrospinning. A purpose-made electrospinning setup, which consisted of a spinneret with a metal needle nozzle, a high voltage power supply, and a special collector, was used to fabricate nanofiber conduits. Figure 1A illustrates the collector. Two conductive magnetic rods (b) were set on the two ends of a short glass rod (a). The magnets were driven to rotate by a transfer system (c) connected with a motor (d). Before electrospinning, a thin layer of molten sugar was dip-coated onto the glass rod so that the fibrous conduits could be easily separated from the rod. Electrospinning was performed by loading a polymer solution into the syringe and then charging the solution with 20 kV DC voltage. The flow rate of polymer solution was controlled by a syringe pump at 0.8 mL/h, and the distance between the needle nozzle and the glass rod collector was controlled at 20 cm. During electrospinning, the rotation speed of the glass rod was 5 rpm. To prove the spinning ability, we also used other polymers such as

DOI: 10.1021/am509227t
ACS Appl. Mater. Interfaces 2015, 7, 7189−7196

PCL, PEU, and PLGA to prepare longitudinally aligned nanofiber conduits.

Characterizations. Fiber morphologies were observed under a field emission scanning electron microscope (FE-SEM, Zeiss SUPRA 55VP). A modified two-dimensional fast Fourier transform (2D FFT) method was adopted to measure the fiber alignment.[15,34]

Implantation. Totally, 36 adult, male Sprague−Dawley rats (230−250g) were randomly divided into three experimental groups with 12 rats in each group. The rats were kept in a humidity and temperature-controlled room, with 12 h light/dark cycles. Standard rat chow and water were supplied sufficiently. All experiments were conducted in accordance with Jiaotong University of Shanghai Institutional Animal Care and used guidelines which were ethically permitted by the Animal Experimental Committee of Sixth People's Hospital affiliated to School of Medicine, Shanghai Jiaotong University.

Two nanofiber-based NGC groups, one with smooth CAB fibers and another with grooved CAB fibers, and one autograft group were used as conduits, which were all 15 mm in length with an inner diameter of 1.5 mm. They were sterilized in ethanol for 2 h before transplantation.

All rats were deeply anesthetized by intra peritoneal sodium pentobarbital (45 mg/kg), and the hair on the right femur was removed before surgery. Under aseptic conditions, a 3 cm incision was made at the right thigh. After splitting dorsolateral gluteal muscles, the sciatic nerve was carefully isolated and exposed from inter muscular space. With the help of an operating microscope, the right sciatic nerve was transected from the popliteal center to the lower edge of piriformis. A 13 mm nerve segment was transected and removed; then, a 15 mm conduit was implanted by interposing the proximal and distal stumps into both ends of the tube (1 mm for each end), followed by suturing with 9/0 monofilament (Ethicon, UK). For the autograft group, a 13 mm segment of the right sciatic nerve was resected, reversed, and sutured back across the nerve defect under perfect microsurgery technology. Finally, the surgical incision was subsequently sutured in layers. To evaluate the function of the nerve regeneration, the animals were sacrificed by cervical dislocation at different time points.

Electrophysiological Analysis. Electrosphysiological analysis was conducted using a previously developed method.[35] An electromyograph machine (Esaote, MYTO, Italy) was used to measure all experimental rats prior to sacrifice at 6 and 12 weeks of implantation. The recordings were taken carefully from the gastrocnemius muscle to avoid false signals. Each rat was anesthetized with sodium pentobarbital, and the regenerated sciatic nerve was exposed by splitting the NGCs in all of the groups. A bipolar stimulating electrode was placed on proximal and distal ends of the regenerated nerves. A monopolar recording electrode was placed in the gastrocnemius muscle. Nerve conduction velocity (NCV) across the regenerated nerve and distal compound motor action potentials (DCMAP) were recorded (n = 6 at week 6 and week 12). The difference in latency and peak amplitude of DCMAP was calculated.

Triple Immunofluorescence. After 12 weeks of implantation, the cross-sectional views of regenerated nerves at the middle of the tubes were visualized by triple immunofluorescence. The regenerated sciatic nerves were fixed with 2.5 v/v % glutaraldehyde in 0.1 M phosphate buffer solution (PBS, pH = 7.4) at 4 °C for 48 h. The samples were then postfixed with 1% osmium tetroxide, dehydrated, and embedded in Epon 812 (Electron Microscopy Sciences, Hatifield, PA) resin. After cutting a thin layer of the embedded nerves (Leica EM UC6 ultramicrotome), mouse antineurofilament 200 (1:1000, Sigma, UK), mouse anti-P0 (1:3000, Astexx, Austria), and Alexa Fluor 586 (1:100) were used to stain the axons and peripheral myelin. Cell nuclei were counter stained with 0.1% of 4,6-diamidino-2-phenylindole (DAPI). The stained sections were rinsed, mounted under coverslips, and viewed on a Zeiss confocal laser scanning microscope (Leica TCS SP5). Quantitative measurement of axons (n = 6) was undertaken using the method described in ref 36.

Immunohistological Assessment. The embedded nerves were circumferentially and longitudinally cut at the middle for immunohistological assessment. Nerve sections were examined for S100 and neurofilament expression by immunohistochemistry using anti-S100 (1:150, Invitrogen, Carlsbad, CA) and rabbit antineurofilament 200 (NF200) antibodies (1:80, Sigma, USA). The mean percentages of S100 positive area ((positive area/intra fascicular area) × 100%) and NF200 positive area ((positive area/intra fascicular area) × 100%) were calculated from the images of circumferential sections (n = 6).

Thin circumferential sections at a thickness of 1 μm were taken (Leica EM UC6 ultra microtome) and stained with 1% toluidine blue. Images were acquired under an oil lens by an optical microscope (Olympus, Model DP72, Japan) and measured by the image analysis program *Image-Pro Plus 6.0* (Media Cybernetics, USA). Randomly selected images of a specimen (n = 3) for each group were analyzed. Myelinated nerve fiber density was calculated by counting the myelinated nerve fibers in the acquired image compared to the image area. Ultrathin sections of 70 nm in thickness were prepared using an ultramicrotome placed on copper grids, stained with lead citrate, and examined by transmission electron microscopy (TEM, CM120, Philips, Netherlands). The diameter of the axons and thickness of the myelin sheath were measured on the basis of the acquired images (n = 6).

Walking Track Analysis. The walking behavior of rats was evaluated to measure the nerve recovery. After implantation for 2, 4, 8, and 12 weeks, the walking track was analyzed by measuring the SFI (n = 6) using a method described in the literature.[37] Briefly, the sciatic function index (SFI, n = 6) was calculated as SFI = ((−38.3 × (EPL − NPL))/NPL) + ((109.5 × (ETS − NTS))/NTS) + ((13.3(EITS − NITS))/NITS) − 8.8. EPL (operated experimental paw length), NPL (normal paw length), ETS (operated experimental toe spread, i.e., distance between the first and fifth toes), NTS (the normal toe spread), EIT (the operated experimental intermediary toe spread, i.e., the distance between the second and the fourth toes), and NIT (normal intermediary toe spread) were measured by an independent investigator who was blinded to the experiments.

Gastrocnemius Muscle Analysis. The bilateral gastrocnemius muscles were removed and weighed on an analytic scale (Hangping, Shanghai, China) at week 12 postsurgery, and the ratio of gastrocnemius muscle weight on the operated side vs the normal side was determined in each group to assess the extent of denervation-induced muscle atrophy (n = 6). Then, the middle portion of the muscle was dissected and placed in 4% paraformaldehyde for hematoxylin and eosin (HE) staining.

Statistical Analysis. Statistical analysis was performed using LSD analysis of variance (ANOVA). Values were averaged and expressed as means ± standard deviation. Statistical analysis was performed using SPSS 13.0 software (SPSS Inc., Chicago, IL), with significance set at $^*p < 0.05$.

RESULTS AND DISCUSSION

Fabrication of the Conduits. During electrospinning, nanofibers were deposited continuously between the ends of two rotary mandrels to form a fibrous tube. When the two mandrels were set in a long distance, a fiber bundle resulted instead of a fibrous tube. This happened due to the collapse of the fibrous tube during electrospinning. Video 1 (am509227t_si_002.avi) in the Supporting Information illustrates the tube collapse during preparation. We have solved this issue by connecting the two mandrels with a coaxial glass rod (Figure 1A). The glass rod was found to effectively prevent the tube from collapsing, ensuring the formation of a tubular structure (Supporting Information, video 2, am509227t_si_003.avi). Here, two electrically conductive magnetic rods were placed at the end of the mandrels. The magnets were used to facilitate fiber alignment because of the local magnetic fields generated.[38,39]

It was noted that it was hard to remove the prepared fibrous tube from the glass rod if the glass rod was used without any treatment. The strong adhesion between the fibers and the rod

DOI: 10.1021/am509227t
ACS Appl. Mater. Interfaces 2015, 7, 7189−7196

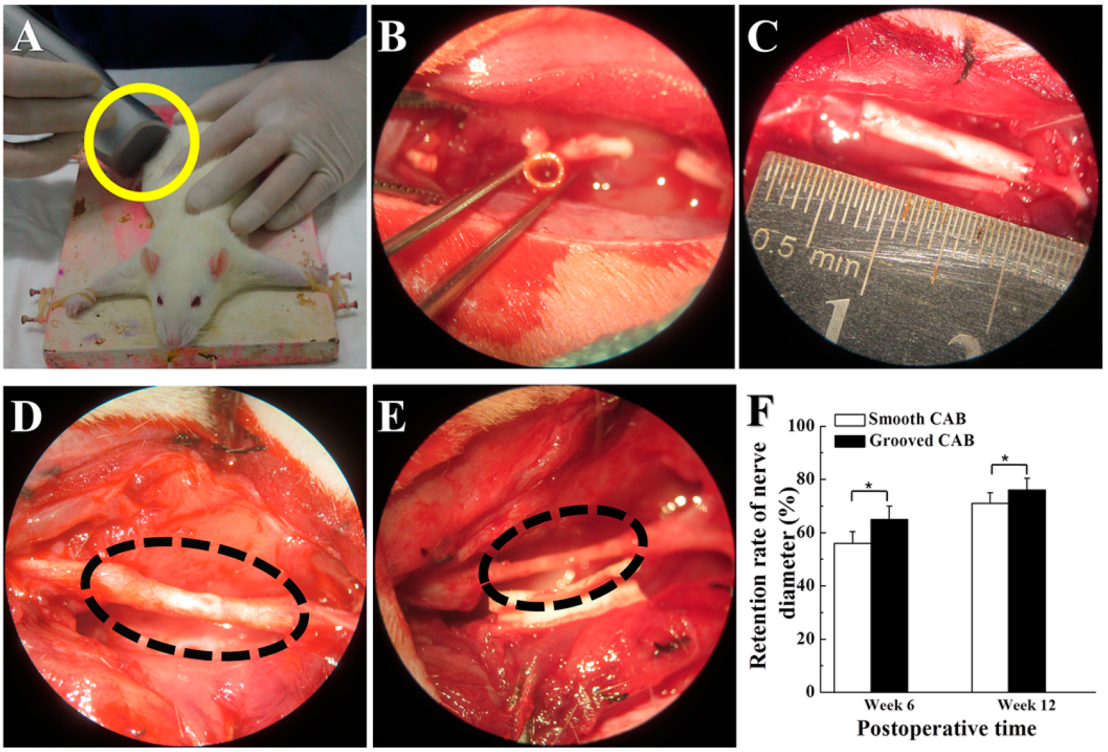

Figure 2. Surgical implantation of nanofiber conduits in a rat sciatic nerve model: (A) shaving the right femur of the experimental rats; (B) photo of conduits before implantation and (C) photo of CAB conduit after bridging the nerve defect; (D) photo of the conduit and (E) the regenerated nerve after 6 weeks of implantation. The oval frames in E and F highlight the regenerated nerve. (F) Statistical analysis of the retention rate of nerve diameter at week 6 and week 12.

came from the static interaction. This problem was solved by coating a thin layer of molten sugar onto the glass rod before electrospinning. In this way, the fibrous tube was released readily by dissolving the sugar layer with water after electrospinning. Here, sugar was selected because of the nontoxicity nature. Sugar is not harmful to cells or tissues even if its removal from the tube is incomplete. This method can be used to prepare aligned fibrous tubes up to 50 mm in length, and the tube diameter can be adjusted through changing the diameter of the glass rod.

Figure 1B shows a digital photo and SEM images of the prepared fibrous CAB conduits. Fibers on both the outer and the inner walls were aligned along the longitudinal direction of the conduit. FFT analysis showed that the fibers on the inner surface had a slightly better alignment than those on the outer surface. Two peaks at around 5° and 185° indicated the direction of fiber alignment along the conduit axis. We also used different polymers, i.e., PLGA, PCL, and PEU, to electrospin longitudinally aligned nanofiber conduits (see SEM images in the Supporting Information, Figure S1). All conduits showed a similar morphology regardless of polymer type, indicating that the method is general, suitable for different polymer materials.

Morphology of CAB Fibers. Figure 1C–E shows the morphology of CAB fibers prepared using CAB with different molecular weights. Although the polymer solutions were in the same solvent system (acetone/DMF), the one from the higher CAB molecular weight ($M_w \sim 70\,000$) resulted in longitudinal grooves on the fiber surface, while the fibers electrospun from the solution of lower molecular weight CAB ($M_w \sim 30\,000$) had a smooth surface. The grooved fibers had an average diameter of ~500 nm, and the grooves were about 200 nm in width (Figure 2E). The smooth fibers had an average diameter of 500 nm, which is similar to that of the grooved fibers.

The mechanism for the formation of surface grooves on electrospun fibers has been elucidated in our previous paper.[32] In brief, voids were formed on the jet surface at the initial stage of electrospinning, and the subsequent elongation and solidification of the voids resulted in the formation of a groove on the fiber surface. The fast evaporation of a highly volatile solvent from the polymer solution plays a key role in the formation of surface voids, while the high viscosity of the residual solution after the solvent evaporation ensured that the grooved surface was maintained after the solidification. We also found that the grooved nanofibers were formed mainly from a polymer with high molecular weight. Fibers with a smooth surface resulted when the molecular weight was low, even if the same type of polymer was used. The high similarity in chemical composition and fiber diameter between the grooved and smooth CAB fibers has provided a promising model to examine the influence of fiber surface morphology on nerve regeneration.

***In Vivo* Nerve Regeneration.** The effect of fiber surface morphology on nerve regeneration of fibrous conduits was studied by an *in vivo* test. Figure 2 shows a typical procedure of implanting CAB conduits to rats. Nerve ends were each sutured over a distance of 1 mm into a 15 mm NGC (Figure 2A–C). Figure 2D shows the same conduit which is covered by native tissues. Both the proximal and distal ends were found to be connected successfully by regenerated nerves (Figure 2E), indicating the efficacy of CAB conduits. After 6 weeks of implantation, a significant difference in the diameter of the regenerated nerves was found on the two groups (Figure 2F). At week 6, the nerve diameter for the smooth conduit and the

DOI: 10.1021/am509227t
ACS Appl. Mater. Interfaces 2015, 7, 7189–7196

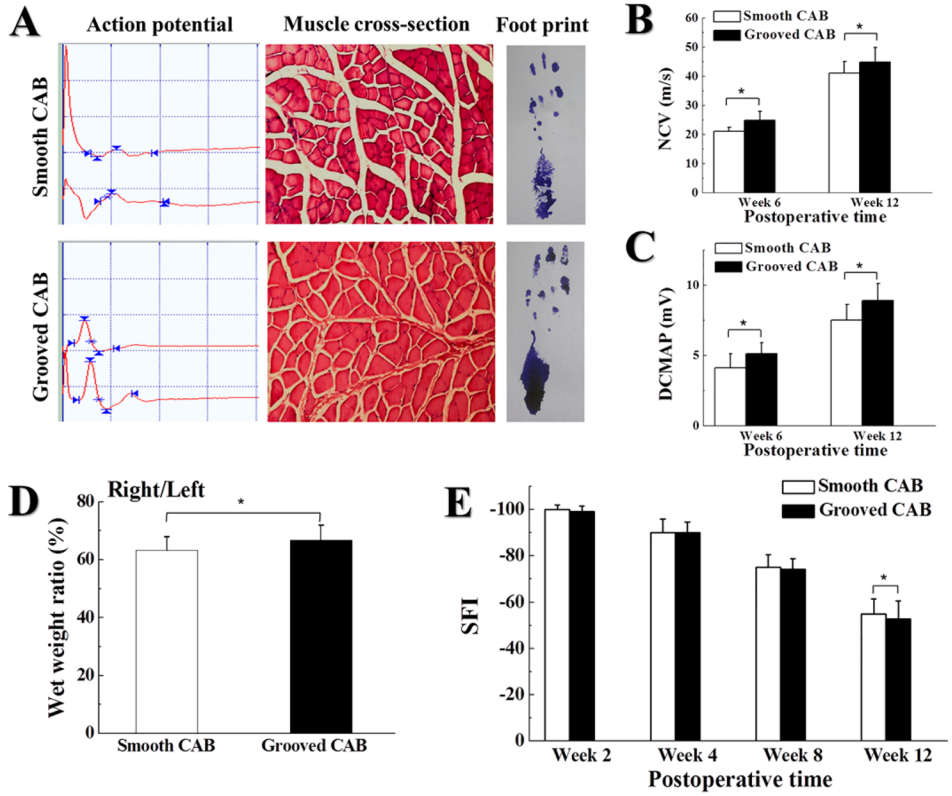

Figure 3. (A) Representative nerve and muscle compound action potentials, typical HE stained cross sections of gastrocnemius muscle, and typical photographs of rat foot prints at week 12 after implantation, (B) NCV and (C) DCMAP from regenerated nerves in rats (5 mV/unit), (D) quantitative analysis of wet weight ratio, and (E) mean SFI calculated from walking track prints at different time spots.

surface-grooved fibrous conduit groups was 56% and 65% of the original size, respectively. At week 12, the corresponding diameter increased to 71% and 76%.

Electrophysiological, gastrocnemius muscle, and walking track analyses were employed to study the recovery behavior. Typical images are shown in Figure 3A. NCV is an objective index to evaluate the conduction of action potential in peripheral nerves,[40] and DCMAP is often used to reflect the numbers of regenerated motor nerve fibers and the extent of muscle.[41] Electrophysiological assessment in Figure 3B,C indicated that the grooved CAB group was significantly higher in both NCV and DCMAP when compared to the smooth CAB group. At week 6, the conduits with grooved fibers had a NCV value of 24.9 m/s and a DCMAP of 5.1 mV, each was ~20% higher than that of the conduits with smooth fibers (21.1 m/s and 4.1 mV). However, at week 12, the difference in NCV and DCMAP between the two groups became less apparent (~15% higher than the grooved CAB group).

When a muscle is denervated as a consequence of nerve injury, the size of the muscle cells would be reduced due to the tendency of muscle degradation.[42] The cross-sectional area of the gastrocnemius muscle in the grooved CAB group was larger than that of the smooth CAB group. NGCs made of grooved CAB successfully prevented the muscle from seriously losing the weight. The quantitative analysis of muscle weight revealed a significant difference between the groups. As shown in Figure 3D, the muscle atrophy after the nerve injury is rescued to a large extent. Walking footprints and SFI from walking track analysis showed a similar trend (Figure 3E). SFI usually oscillates around 0 for normal nerve function, whereas that at around −100 represents total dysfunction. After transaction, the nerve conduction pathway was completely destroyed. SFI in the CAB groups decreased dramatically at the beginning weeks with no NCV being detected. In the following weeks, the value constantly increased with time. In comparison with the smooth CAB group, the grooved CAB group had higher SFI since week 8. The difference became more significant at week 12.

Triple immunofluorescence provides a general view of the nerve structure. As shown in Figure 4A, the density of neurofilaments in the grooved CAB group was higher than that of the smooth CAB group. Quantitative results indicated that the area of myelinated axons in the smooth fiber conduits was 83.8% of the area in the grooved conduits. Figure 4B,C shows visualized proofs from immunohistological analyses in which circumferential and longitudinal sections of the conduits were stained by S-100 and NF200. The circumferential view indicated more cells in the grooved CAB group. The longitudinal sections revealed that Schwann cells in both the grooved and the smooth fiber groups grew along the longitudinal direction of the nerves, and the cells on the grooved CAB conduits had better alignment than those on the smooth CAB conduits. Similarly, the grooved CAB conduits had better axonal recovery. Statistical results at week 6 indicated that both S100 and NF200 positive areas of the grooved CAB conduits were ~18% larger than those of the smooth conduits.

Toluidine blue and TEM images indicated that more myelin sheaths and axons with uniform size were formed on the grooved CAB conduits (Figure 4D). This suggested that the surface grooves assisted in formation of neuro-filament. The diameter of axons and thickness of myelin sheath in the grooved CAB conduits were larger than those in the smooth

DOI: 10.1021/am509227t
ACS Appl. Mater. Interfaces 2015, 7, 7189−7196

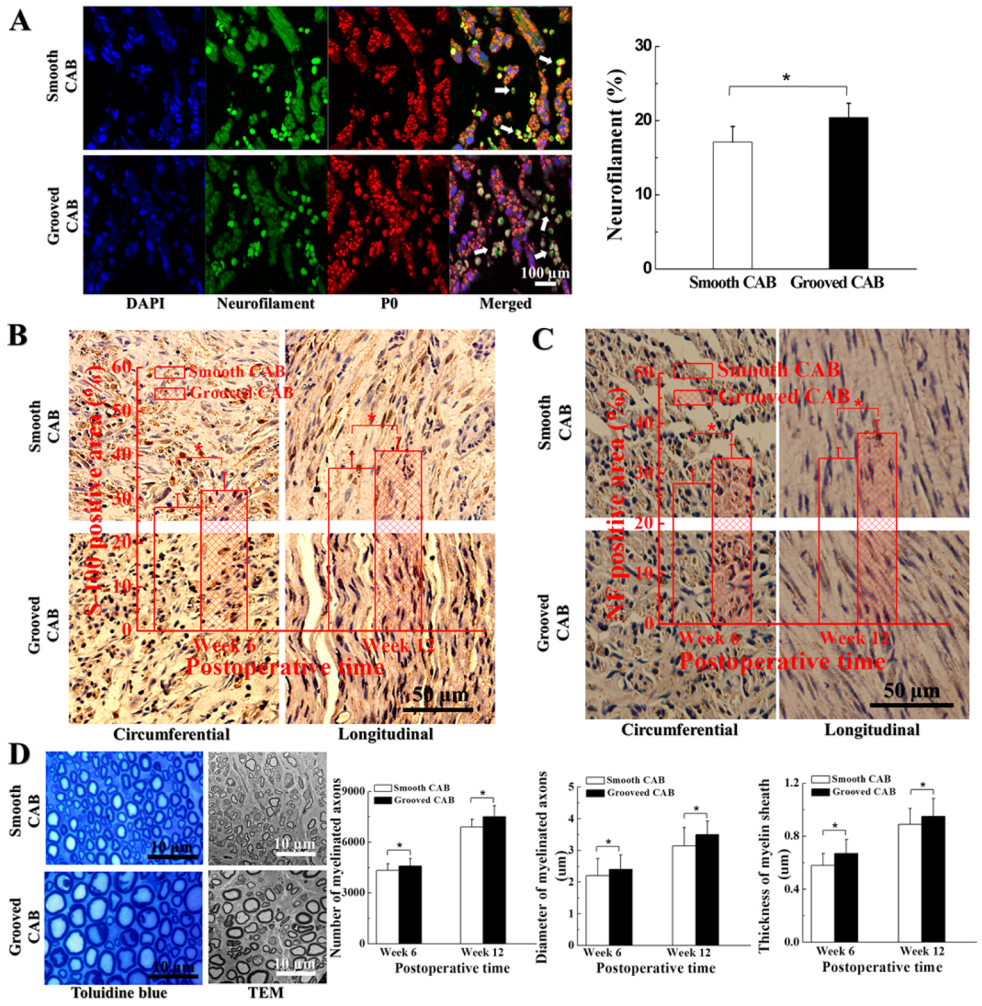

Figure 4. (A) Triple immunofluorescence for the cross sections of sciatic nerves after 12 weeks of implantation: DAPI (cell nuclei, blue), neurofilament (axon, green), and P0 (myelin, red) and percentage of neurofilaments in the area. Typical myelinated axons are marked by white arrows in the merged images; (B) immunohistological analysis of regenerated nerve sections stained with an antibody to the Schwann cell marker S-100 and percentage of S-100 positive area in the circumferential nerve sections; (C) regenerated nerve sections stained with an antibody to neuronal NF200 and percentage of NF positive area in the circumferential nerve sections; (D) myelination of regenerated nerves revealed by toluidine blue and TEM, statistical analysis of the number of myelinated axons, diameter of myelinated axons, and thickness of myelin sheath at week 12 after implantation.

CAB conduits, suggesting better nerve regrowth for the grooved CAB conduit group in both quantity and quality. It should be noted that all significant differences occurred at week 6, which was consistent with the NCV and DCMAP results. Therefore, grooved nanofibers had a positive effect on peripheral nerve regeneration.

Aligned nanofibers can offer a highly oriented surface structure. As illustrated in Figure 5, the grooves on the fibers

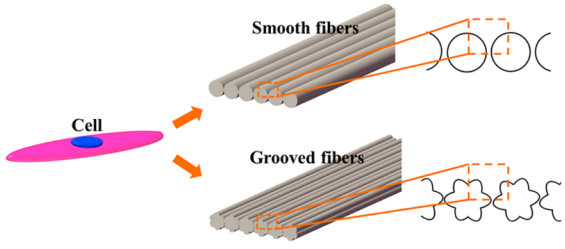

Figure 5. Schematic diagram of the scaffold formed by the aligned fibers having a smooth and grooved surface for cell seeding.

added a secondary aligned structure, making the aligned fiber surface have finer feature. As cells can recognize nanosized texture with a feature size much smaller than cell dimension,[43,44] the surface grooves formed by aligned nanofibers could effectively enhance the linear cell growth and the elongation of the cytoskeleton.

In our previous paper, we have analyzed the effect of surface grooves on fiber surface area. The fiber surface area increases with an increase in the groove number. For CAB fibers, on average, 6 grooves were found on each fiber. The fiber surface area was estimated to increase by up to 20%.[32] Such an increase in the surface area could lead to improved cell adhesion and proliferation.[45]

For comparison, an autograft was also used for the *in vivo* test (see the results in Supporting Information, Figure S3, Tables S1 and S2). The autograft group showed a better nerve recovery than the nanofiber groups. The retention rate of the diameter of regenerated nerves in the autograft was 82% and 90%, respectively, at weeks 6 and 12. Although autologous sciatic nerve segments were reversed before suturing back, most of the neurofilaments and axons in these segments were able to

DOI: 10.1021/am509227t
ACS Appl. Mater. Interfaces 2015, 7, 7189−7196

reserve their original function. Reasons for the better nerve recovery of autograft is because of the presence of neurofilaments in the autograft conduit. For the nanofiber conduits, nerve function had to be reconstructed thoroughly, due to the absence of neurofilaments and axons before implantation, resulting in a longer recovery period than the autograft. Nevertheless, most of the differences between the grooved and the smooth fiber conduits were still statistically significant even if the autograft group is included.

CONCLUSIONS

We have prepared fibrous conduits from aligned nanofibers. By forming longitudinal grooves on the nanofiber surface, we have found that the conduit shows considerable improvement in nerve regeneration. This is mainly attributed to the highly ordered secondary structure formed by surface grooves and an increase in the specific surface area. Our study indicates that fibrous conduits made of longitudinally aligned nanofibers, which have longitudinal nanogrooves on the fiber surface, may offer a new NGC for nerve repair and regeneration.

ASSOCIATED CONTENT

Supporting Information

Videos of conduit fabrication, images of longitudinally aligned fibrous conduits from various polymers, and *in vivo* results of autograft group. This material is available free of charge via the Internet at http://pubs.acs.org.

AUTHOR INFORMATION

Corresponding Authors

*E-mail: ouyangyuanming@163.com.
*E-mail: tong.lin@deakin.edu.au.

Author Contributions

C. Huang and H. Niu designed the electrospinning setup. C. Huang fabricated the fiber conduits, conducted materials characterization, and drafted the manuscript. Y. Ouyang conducted the *in vivo* study and analyzed the test results. H. Niu built the electrospinning setup. N. He measured the alignment of fibers. Q. Ke and X. Jin analyzed the material related experimental results. D. Li and J. Fang performed the cell culture and confocal microscopy imaging. W. Liu and C. Fan conducted immunohistological test and result analysis. T. Lin worked on all aspects of the work, including designing experiments, supervising researchers, result analysis, and finalizing the manuscript. All authors contributed to revision of the manuscript.

Notes

The authors declare no competing financial interest.

ACKNOWLEDGMENTS

Financial support by the Fundamental Research Funds for the Central Universities (2232014D3-15), National Natural Science Foundation of China (51403033 and 81171477), the Science and Technology Commission of Shanghai Municipality (11JC1409800), and Funds for Interdisciplinary Projects of Medicine and Engineering by Shanghai Jiaotong University (YG2013MS52) are acknowledged.

REFERENCES

(1) Cao, H.; Liu, T.; Chew, S. Y. The Application of Nanofibrous Scaffolds in Neural Tissue Engineering. *Adv. Drug Delivery Rev.* **2009**, *61*, 1055−1064.
(2) Schmidt, C. E.; Leach, J. B. Neural Tissue Engineering: Strategies for Repair and Regeneration. *Annu. Rev. Biomed. Eng.* **2003**, *5*, 293−347.
(3) Jiang, X.; Lim, S. H.; Mao, H. Q.; Chew, S. Y. Current Applications and Future Perspectives of Artificial Nerve Conduits. *Exp. Neurol.* **2010**, *223*, 86−101.
(4) Lu, W.; Sun, J.; Jiang, X. Recent Advances in Electrospinning Technology and Biomedical Applications of Electrospun Fibers. *J. Mater. Chem. B* **2014**, *2*, 2369−2380.
(5) He, X.; Xiao, Q.; Lu, C.; Wang, Y.; Zhang, X.; Zhao, J.; Zhang, W.; Zhang, X.; Deng, Y. Uniaxially Aligned Electrospun All-Cellulose Nanocomposite Nanofibers Reinforced with Cellulose Nanocrystals: Scaffold for Tissue Engineering. *Biomacromolecules* **2014**, *15*, 618−627.
(6) He, L.; Liao, S.; Quan, D.; Ngiam, M.; Chan, C. K.; Ramakrishna, S.; Lu, J. The Influence of Laminin-Derived Peptides Conjugated to Lys-Capped Plla on Neonatal Mouse Cerebellum C17.2 Stem Cells. *Biomaterials* **2009**, *30*, 1578−1586.
(7) Kim, J. R.; Oh, S. H.; Kwon, G. B.; Namgung, U.; Song, K. S.; Jeon, B. H.; Lee, J. H. Acceleration of Peripheral Nerve Regeneration through Asymmetrically Porous Nerve Guide Conduit Applied with Biological/Physical Stimulation. *Tissue Eng., Part A* **2013**, *19*, 2674−2685.
(8) Bettinger, C. J.; Langer, R.; Borenstein, J. T. Engineering Substrate Topography at the Micro- and Nanoscale to Control Cell Function. *Angew. Chem., Int. Ed.* **2009**, *48*, 5406−5415.
(9) Yao, X.; Peng, R.; Ding, J. Cell-Material Interactions Revealed via Material Techniques of Surface Patterning. *Adv. Mater.* **2013**, *25*, 5257−5286.
(10) Yan, C.; Sun, J.; Ding, J. Critical Areas of Cell Adhesion on Micropatterned Surfaces. *Biomaterials* **2011**, *32*, 3931−3938.
(11) Wrobel, M. R.; Sundararaghavan, H. G. Directed Migration in Neural Tissue Engineering. *Tissue Eng., Part B* **2014**, *20*, 93−105.
(12) Zhao, S.; Zhou, Q.; Long, Y.-Z.; Sun, G.-H.; Zhang, Y. Nanofibrous Patterns by Direct Electrospinning of Nanofibers onto Topographically Structured Non-Conductive Substrates. *Nanoscale* **2013**, *5*, 4993−5000.
(13) Langer, R.; Vacanti, J. P. Tissue Engineering. *Science* **1993**, *260*, 920−926.
(14) Katta, P.; Alessandro, M.; Ramsier, R. D.; Chase, G. G. Continuous Electrospinning of Aligned Polymer Nanofibers onto a Wire Drum Collector. *Nano Lett.* **2004**, *4*, 2215−2218.
(15) Parker, A. R.; Lawrence, C. R. Water Capture by a Desert Beetle. *Nature* **2001**, *414*, 33−34.
(16) Xie, J.; Liu, W.; MacEwan, M. R.; Bridgman, P. C.; Xia, Y. Neurite Outgrowth on Electrospun Nanofibers with Uniaxial Alignment: The Effects of Fiber Density, Surface Coating, and Supporting Substrate. *ACS Nano* **2014**, *8*, 1878−1885.
(17) Lim, S. H.; Liu, X. Y.; Song, H.; Yarema, K. J.; Mao, H. Q. The Effect of Nanofiber-Guided Cell Alignment on the Preferential Differentiation of Neural Stem Cells. *Biomaterials* **2010**, *31*, 9031−9039.
(18) Yucel, D.; Kose, G. T.; Hasirci, V. Tissue Engineered, Guided Nerve Tube Consisting of Aligned Neural Stem Cells and Astrocytes. *Biomacromolecules* **2010**, *11*, 3584−3591.
(19) Zheng, Y.; Gao, X.; Jiang, L. Directional Adhesion of Superhydrophobic Butterfly Wings. *Soft Matter* **2007**, *3*, 178−182.
(20) Chew, S. Y.; Mi, R.; Hoke, A.; Leong, K. W. Aligned Protein−Polymer Composite Fibers Enhance Nerve Regeneration: A Potential Tissue-Engineering Platform. *Adv. Funct. Mater.* **2007**, *17*, 1288−1296.
(21) Kim, Y.-t.; Haftel, V. K.; Kumar, S.; Bellamkonda, R. V. The Role of Aligned Polymer Fiber-Based Constructs in the Bridging of Long Peripheral Nerve Gaps. *Biomaterials* **2008**, *29*, 3117−3127.
(22) Huang, W.; Begum, R.; Barber, T.; Ibba, V.; Tee, N. C. H.; Hussain, M.; Arastoo, M.; Yang, Q.; Robson, L. G.; Lesage, S.; Gheysens, T.; Skaer, N. J. V.; Knight, D. P.; Priestley, J. V. Regenerative Potential of Silk Conduits in Repair of Peripheral Nerve Injury in Adult Rats. *Biomaterials* **2012**, *33*, 59−71.

DOI: 10.1021/am509227t
ACS Appl. Mater. Interfaces 2015, 7, 7189−7196

(23) de Groot, B. L.; Grubmüller, H. Water Permeation across Biological Membranes: Mechanism and Dynamics of Aquaporin-1 and Glpf. *Science* **2001**, *294*, 2353−2357.
(24) Wheeler, T. D.; Stroock, A. D. The Transpiration of Water at Negative Pressures in a Synthetic Tree. *Nature* **2008**, *455*, 208−212.
(25) Jana, S.; Zhang, M. Fabrication of 3d Aligned Nanofibrous Tubes by Direct Electrospinning. *J. Mater. Chem. B* **2013**, *1*, 2575−2581.
(26) Xie, J.; MacEwan, M. R.; Schwartz, A. G.; Xia, Y. Electrospun Nanofibers for Neural Tissue Engineering. *Nanoscale* **2010**, *2*, 35−44.
(27) Francel, P. C.; Smith, K. S.; Stevens, F. A.; Kim, S. C.; Gossett, J.; Gossett, C.; Davis, M. E.; Lenaerts, M.; Tompkins, P. Regeneration of Rat Sciatic Nerve across a Lactosorb Bioresorbable Conduit with Interposed Short-Segment Nerve Grafts. *J. Neurosurg.* **2003**, *99*, 549−554.
(28) Gertz, C. C.; Leach, M. K.; Birrell, L. K.; Martin, D. C.; Feldman, E. L.; Corey, J. M. Accelerated Neuritogenesis and Maturation of Primary Spinal Motor Neurons in Response to Nanofibers. *Dev. Neurobiol.* **2010**, *70*, 589−603.
(29) Ahmed, Z.; Brown, R. A. Adhesion, Alignment, and Migration of Cultured Schwann Cells on Ultrathin Fibronectin Fibres. *Cell Motil. Cytoskeleton* **1999**, *42*, 331−343.
(30) Manwaring, M. E.; Walsh, J. F.; Tresco, P. A. Contact Guidance Induced Organization of Extracellular Matrix. *Biomaterials* **2004**, *25*, 3631−3638.
(31) Curtis, A. S. G.; Casey, B.; Gallagher, J. O.; Pasqui, D.; Wood, M. A.; Wilkinson, C. D. W. Substratum Nanotopography and the Adhesion of Biological Cells. Are Symmetry or Regularity of Nanotopography Important? *Biophys. Chem.* **2001**, *94*, 275−283.
(32) Huang, C.; Tang, Y.; Liu, X.; Sutti, A.; Ke, Q.; Mo, X.; Wang, X.; Morsi, Y.; Lin, T. Electrospinning of Nanofibres with Parallel Line Surface Texture for Improvement of Nerve Cell Growth. *Soft Matter* **2011**, *7*, 10812−10817.
(33) Fundueanu, G.; Constantin, M.; Esposito, E.; Cortesi, R.; Nastruzzi, C.; Menegatti, E. Cellulose Acetate Butyrate Microcapsules Containing Dextran Ion-Exchange Resins as Self-Propelled Drug Release System. *Biomaterials* **2005**, *26*, 4337−4347.
(34) Zhou, H.; Wang, H.; Niu, H.; Lin, T. Superphobicity/Philicity Janus Fabrics with Switchable, Spontaneous, Directional Transport Ability to Water and Oil Fluids. *Sci. Rep.* **2013**, *3*, 2964.
(35) Wang, C.-Y.; Zhang, K.-H.; Fan, C.-Y.; Mo, X.-M.; Ruan, H.-J.; Li, F.-F. Aligned Natural−Synthetic Polyblend Nanofibers for Peripheral Nerve Regeneration. *Acta Biomater.* **2011**, *7*, 634−643.
(36) Daniel, S.; Chaudhury, M. K.; Chen, J. C. Fast Drop Movements Resulting from the Phase Change on a Gradient Surface. *Science* **2001**, *291*, 633−636.
(37) Cao, J.; Sun, C.; Zhao, H.; Xiao, Z.; Chen, B.; Gao, J.; Zheng, T.; Wu, W.; Wu, S.; Wang, J.; Dai, J. The Use of Laminin Modified Linear Ordered Collagen Scaffolds Loaded with Laminin-Binding Ciliary Neurotrophic Factor for Sciatic Nerve Regeneration in Rats. *Biomaterials* **2011**, *32*, 3939−3948.
(38) Liu, K.; Yao, X.; Jiang, L. Recent Developments in Bio-Inspired Special Wettability. *Chem. Soc. Rev.* **2010**, *39*, 3240−3255.
(39) Domingues, R. M. A.; Gomes, M. E.; Reis, R. L. The Potential of Cellulose Nanocrystals in Tissue Engineering Strategies. *Biomacromolecules* **2014**, *15*, 2327−2346.
(40) Toyoshima, E.; Yeager, A. M.; Brennan, S.; Santos, G. W.; Moser, H. W.; Mayer, R. F. Nerve Conduction Studies in the Twitcher Mouse (Murine Globoid Cell Leukodystrophy). *J. Neurol. Sci.* **1986**, *74*, 307−318.
(41) Vucic, S.; Black, K.; Tick Chong, P. S.; Cros, D. Multifocal Motor Neuropathy with Conduction Block: Distribution of Demyelination and Axonal Degeneration. *Clin. Neurophysiol.* **2007**, *118*, 124−130.
(42) Sola, O. M.; Christensen, D. L.; Martin, A. W. Hypertrophy and Hyperplasia of Adult Chicken Anterior Latissimus Dorsi Muscles Following Stretch with and without Denervation. *Exp. Neurol.* **1973**, *41*, 76−100.
(43) Angarano, M.; Schulz, S.; Fabritius, M.; Vogt, R.; Steinberg, T.; Tomakidi, P.; Friedrich, C.; Mülhaupt, R. Layered Gradient Nonwovens of in Situ Crosslinked Electrospun Collagenous Nanofibers Used as Modular Scaffold Systems for Soft Tissue Regeneration. *Adv. Funct. Mater.* **2013**, *23*, 3277−3285.
(44) Goto, M.; Tsukahara, T.; Sato, K.; Kitamori, T. Micro- and Nanometer-Scale Patterned Surface in a Microchannel for Cell Culture in Microfluidic Devices. *Anal. Bioanal. Chem.* **2008**, *390*, 817−823.
(45) Park, S. J.; Lee, B. K.; Na, M. H.; Kim, D. S. Melt-Spun Shaped Fibers with Enhanced Surface Effects: Fiber Fabrication, Characterization and Application to Woven Scaffolds. *Acta Biomater.* **2013**, *8*, 7719−7726.

DOI: 10.1021/am509227t
ACS Appl. Mater. Interfaces 2015, 7, 7189−7196